A theoretical investigation of the glide dislocations in the sphalerite ZnS

Lili Huang and Shaofeng Wang[a)]
Department of Physics and Institute for Structure and Function, Chongqing University, Chongqing 400030, People's Republic of China

The 90° and 30° partial glide dislocations in ZnS are investigated theoretically in the framework of the fully discrete Peierls model and first-principles calculation. It is found that there are four types of equilibrium cores for each kind of partial glide dislocation, which are named as the O-Zn-core, the B-Zn-core, the O-S-core, and the B-S-core, according to their geometrical feature and atomic ingredient at the core. For the 90° partial dislocation, the O-Zn-core (double-period core) and the B-S-core (single-period core) are stable. The Peierls barrier heights of the O-Zn-core and the B-S-core are about 0.03 eV/Å and 0.01 eV/Å, respectively. For the 30° partial dislocation, the O-Zn-core (double-period core) and the B-Zn-core (single-period core) are stable and their Peierls barrier heights are approximately the same as that of the O-Zn-core of the 90° partial dislocation. The Peierls stress related to the barrier height is about 800 MPa for the 90° partial dislocation with the B-S-core. The existence of unstable equilibrium cores enables us to introduce the concept of the partial kink. Based on the concept of the partial kink, a minimum energy path is proposed for the formation and migration of kinks. It is noticed that the step length in kink migration is doubled due to the core reconstruction. *Published by AIP Publishing.* https://doi.org/10.1063/1.5050063

I. INTRODUCTION

Recently, extraordinary plasticity of ZnS in darkness was reported and attracted great attention.[1] It was found that ZnS crystals can be plastically deformed up to a deformation strain of $e_t = 45\%$ in complete darkness. In contrast, ZnS crystals immediately fractured when they deformed under light irradiation. Semiconductor ZnS with the sphalerite structure is an important photoelectronic material. The stacking fault energy of ZnS is very low.[2] As a result, the majority of the glide dislocations in ZnS dissociates into the 90° and 30° partial dislocations.[1,3] The pure electric charges at the core was observed for the moving dislocations in ZnS.[4]

In order to understand the plasticity of ZnS, it is necessary to clearly reveal the core structure of an isolated dislocation and the relevant properties. If we know the dislocation cores and their evolution processes with single-atom sensitivity, it can lead to a far greater understanding on the correlation between the dislocation cores and the mechanical, optical, and electronic behaviours. Several experimental techniques exist for probing dislocations, but no one can individually provide sufficient information to the local core structure at the atomic scale.[5] In theory, the core structure can be studied by using classical inter-atomic potentials.[6] However, since these potentials are often unable to reproduce the effects of intrinsic quantum features such as bond breaking and reconstruction, the reliability is a question. The structure can also be studied by using electron-density functional theory.[7–10] However, due to the limitation of calculation ability, the super-cell cannot be large enough to address the large scale problems. Rather than an isolated dislocation, one has to use a dipole cell to eliminate the effects of the long-range

field of the dislocations. Unfortunately, while the problems require that the long-range field be removed, the interaction between the dislocations is introduced as long as the dipole cell is used.

In this paper, following the way presented in Ref. 11, the 90° and 30° partial glide dislocations in ZnS are investigated theoretically in the framework of the fully discrete Peierls model and first-principles calculation. Firstly, the lattice constant, elastic constants, and the γ-potential are studied from the first-principles calculation. Then, the dislocation core structures are investigated in the framework of the fully discrete Peierls model. Finally, with the help of the results obtained in analytical theory, the exact core structures are obtained from relaxation based on the first-principles calculation. Surprisingly, it is found that there are two stable cores for each kind of partial dislocation in ZnS, and every stable core has an unstable core as its partner. The existence of a partner enables us to introduce the concept of the partial kink. Based on the concept of the partial kink, a minimum energy path is proposed to explain the microscopical process in formation and migration of the kinks.

II. THE GLIDE DISLOCATION IN THE FULLY DISCRETE PEIERLS THEORY

The γ-surface (generalized stacking fault energy) is widely used to characterize mechanical properties related to nonlinear phenomena.[6] The γ-surface is defined as the interaction energy between two parallel half-infinite crystals with the fixed space (non-relaxed γ-surface). When a crystal is cut into two half-infinite parts by a given cut-plane, the interaction energy will change when the two parts occur at a relative slip rigid-translation. The interaction energy per unit area as a function of the slip rigid-translation is referred to as the γ-surface of the cut-plane. For the glide dislocations in the

a)E-mail: sfwang@cqu.edu.cn

diamond, sphalerite, or wurtzite structures, the cut-plane is the {111} plane, and the space between the upper half and the lower half is narrow one, $d = \sqrt{3}a_0/12$, where a_0 is the lattice constant. Obviously, when there is a relative slip, the bonds connecting two halves will be strongly compressed if the space is not changed. In order to completely describe the interaction between two halves, the variation of the interaction energy as a function of the space should be taken into account. The γ-surface should be generalized as γ-potential to include the interaction due to space varying.

Generally, γ-potential is defined on a three-dimensional space (rigid-translation space) because a rigid-translation can be parallel or perpendicular to the cut-plane. However, in theoretical study of dislocations, the slip-translation is usually confined to the direction parallel to the Burgers vector. For sphalerite ZnS, it is easy to see that the slip-translations related to the 90° and the 30° partial dislocations are equivalent due to the symmetry of the {111} plane. Thus, the γ-potentials are the same for the 90° and the 30° partial dislocations if the slip is confined to along the Burgers vector.

For consistency, the lattice constant and elastic constant are firstly calculated for ZnS from the electron density functional theory. In Table I, these constants and related parameters are listed. Using the equilibrium structure obtained, the γ-potential of the {111} plane is evaluated from the first-principles calculation in the way described in Ref. 11. In Fig. 1, the γ-potential as a function of the slip along the Burgers vector is plotted for some typical spaces. As usually supposed for ZnS, the stacking fault energy is found to be very low $E_{sf} = 0.001 \, \text{eV/A}^2$. The γ-potential can be expressed by the following analytical formula

$$\gamma(u_b, u_y) = \phi_0 + \gamma_1(u_y)\cos^2\frac{\pi u_b}{b} + \gamma_2(u_y)\cos^4\frac{\pi u_b}{b},$$
$$\gamma_1 = -3\phi_0 - \phi_1 + 4\phi_2, \quad \gamma_2 = 2\phi_0 + 2\phi_1 - 4\phi_2, \quad (1)$$

where u_b describes the slip parallel to the Burgers vector and u_y describes the space change, ϕ_i, is Morse function with an additive constant

$$\phi_i(u_y) = s_i\left(e^{-2\alpha_i(u_y - v_i)/d} - 2e^{-\alpha_i(u_y - v_i)/d}\right) + t_i,$$
$$i = 0, 1, 2. \quad (2)$$

The parameters in ϕ_i are shown in Table II. As seen from Fig. 1, the γ-potential from the first-principles calculation can be well described by the analytical formula.

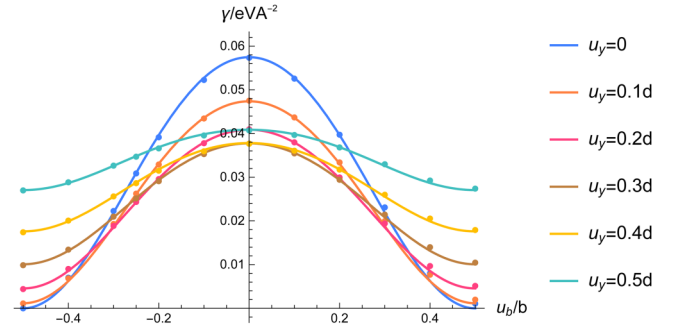FIG. 1. The γ-potential of the (111) plane as a function of the slip along $\langle11\bar{2}\rangle$ direction for some typical spaces, $d + u_y = d$, $1.1d$, $1.2d$, $1.3d$, $1.4d$, $1.5d$, $d = \sqrt{3}a_0/12$ is the lattice space of an ideal crystal. The solid lines are given by the analytical formula and the dots are given by the first-principles calculation. The unstable energy decreases as the distance increases.

One important goal of an analytical theory of dislocations is understanding dislocations from the elementary knowledge of mechanical properties of a crystal. It is the Peierls model that establishes the relationship between the dislocation structure and the properties of a bulk solid.[18,19] Recently, a fully discrete Peierls theory is presented and used to investigate the 90° partial dislocation in silicon.[11] The theory can be generalized to deal with a mixed dislocation by neglecting the small component of the mismatch field.[20] For an arbitrary mixed dislocation, the dislocation equation satisfied by the major component u_b (parallel to the Burgers vector) and space varying u_y is

$$-\frac{\beta_b}{2\lambda^2}[\rho_b(l) - \rho_b(l-1)] - \frac{K_b}{2\pi\lambda}\sum_{l'=-\infty}^{\infty}\frac{\rho_b(l')}{l' - l + \frac{1}{2}} = f_b(l), \quad (3)$$

$$-\frac{K_{e_y}}{2\pi\lambda}\sum_{l'=-\infty}^{\infty}\frac{\rho_y(l')}{l' - l + \frac{1}{2}} = f_y(l), \quad (4)$$

where $\rho_b(l) = u_b(l+1) - u_b(l)$ and $\rho_y(l) = u_y(l+1) - u_y(l)$ are the discrete dislocation densities, $\mathbf{f} = -\nabla\gamma(\mathbf{u})$, and $\lambda = \sqrt{6}a_0/4$ is the distance between the lattice lines paralleled to the dislocation line. The physical constants in the equation are given by

$$\beta_b = \beta\sin^2\theta, \quad \beta = \frac{(c_{11} - c_{12})a_0^3}{16\sigma},$$
$$K_b = K_{e_x}\sin^2\theta + K_s\cos^2\theta,$$

where θ is the angle between the dislocation line and the Burgers vector, σ is the area of the primitive cell of the {111} plane that is a two-dimensional lattice, K_{e_x}, K_{e_y}, and K_s are the energy factors of a mixed dislocation, which are defined in Refs. 21 and 22. In Table I, values of these

TABLE I. The lattice constant a_0 (Å), the elastic constants c_{ij} (GPa), and the parameters appearing in the dislocation equation.

	a_0	c_{11}	c_{12}	c_{44}	β	K_{ex}	K_{ey}	K_s
This work	5.45	95.21	52.64	65.77	3.35	61.81	58.77	37.42
Expt 12	5.41	104.0	65.0	46.2	3.05	49.84	51.51	30.02
Ref. 13	5.34	123.7	62.1	59.7	4.75	63.79	65.77	42.89
Ref. 14	...	104	53.55	50.72	...	53.79	55.53	35.77
Ref. 15	5.40	105.1	67.2	42.7	3.0	47.73	49.18	28.45
Ref. 16	5.34	118.0	72.0	75.0	3.55	69.08	72.52	41.53
Ref. 17	5.40	99.6	57.0	50.5	3.32	51.98	53.90	32.80

TABLE II. The parameters in the γ-potential.

$s_0 = 4.013 \, \text{eV/Å}^2$	$\alpha_0 = 0.171$	$v_0 = 0 \, \text{Å}$	$t_0 = 4.013 \, \text{eV/Å}^2$
$s_1 = 3.431 \, \text{eV/Å}^2$	$\alpha_1 = 0.212$	$v_1 = 0.274 \, \text{Å}$	$t_1 = 3.468 \, \text{eV/Å}^2$
$s_2 = 3.190 \, \text{eV/Å}^2$	$\alpha_2 = 0.209$	$v_2 = 0.170 \, \text{Å}$	$t_2 = 3.215 \, \text{eV/Å}^2$

TABLE III. The parameters in the dislocation solution and the energy E.

		α_b	α_y	c_b	c_y	$\zeta(b)$	$\xi(b)$	$E(eV/\text{Å})$
90°	B-type	0	1/2	0.705	0.089	1.099	0.627	0.245
partial	O-type	1/2	0	0.787	0.109	1.267	0.707	0.257
30°	B-type	0	1/2	0.630	0.034	0.758	0.674	0.176
partial	O-type	1/2	0	0.806	0.108	0.899	0.542	0.219

physical constants are listed for ZnS. The energy functional of the dislocation equations is

$$E = \frac{\beta_b}{4\lambda^2} \sum_{l=-\infty}^{\infty} \rho_b^2(l) - \frac{1}{4\pi\lambda} \sum_{l=-\infty}^{\infty} \sum_{l'=-\infty}^{\infty} [K_b \rho_b(l)\rho_b(l')$$

$$+ K_{e_y}\rho_y(l)\rho_y(l')]\psi^{(0)}(|l - l'| + \frac{1}{2}) + \sum_{l=-\infty}^{\infty} \gamma(u_b, u_y), \quad (5)$$

where $\psi^{(0)}(z)$ is the Polygamma function.[11]

The solutions of the discrete dislocation equations are proposed to be[11]

$$u_b(l) = \frac{\hat{D}u_b^{(0)}}{\hat{D}Q_0}b, \quad u_y = \frac{c_y b\xi}{\xi^2 + (l - \alpha_y)^2\lambda^2}, \quad (6)$$

where $\hat{D}$ is the parametric derivative

$$\hat{D} = (1 - c_b)\bar{\zeta}^2 - c_b\bar{\zeta}^3 \frac{\partial}{\partial\bar{\zeta}}$$

and

$$u_b^{(0)}(l) = \frac{i}{2\bar{\zeta}}[\psi^{(0)}(-l + \alpha_b - i\bar{\zeta} + 1) - \psi^{(0)}$$

$$\times (-l + \alpha_b + i\bar{\zeta} + 1)],$$

$$Q_0 = \frac{\pi}{\bar{\zeta}} \times \frac{\sinh(2\pi\bar{\zeta})}{\cosh(2\pi\bar{\zeta}) - \cos(2\pi t)} \quad \bar{\zeta} = \frac{\zeta}{\lambda}.$$

In the expression of the solution, $\alpha_b = 0$, 1/2 and $\alpha_y = 1/2 - \alpha_b$, labeling the center position of the dislocation distribution, ζ and ξ describe characterized width, and c_b and c_y are structure constants. Using expression (6) as the trial function with the variational parameters ζ, ξ, c_b, and c_y, the approximated solutions are obtained from the Ritz variational method. The final results are shown in Table III, where all the parameters in the solutions of the 90° and 30° partial dislocations are listed. The distributions of dislocation density are shown in Fig. 2

As pointed out already in Ref. 11, for each dislocation, there are two solutions of the dislocation equation. Therefore, a dislocation has two types of equilibrium cores, which are
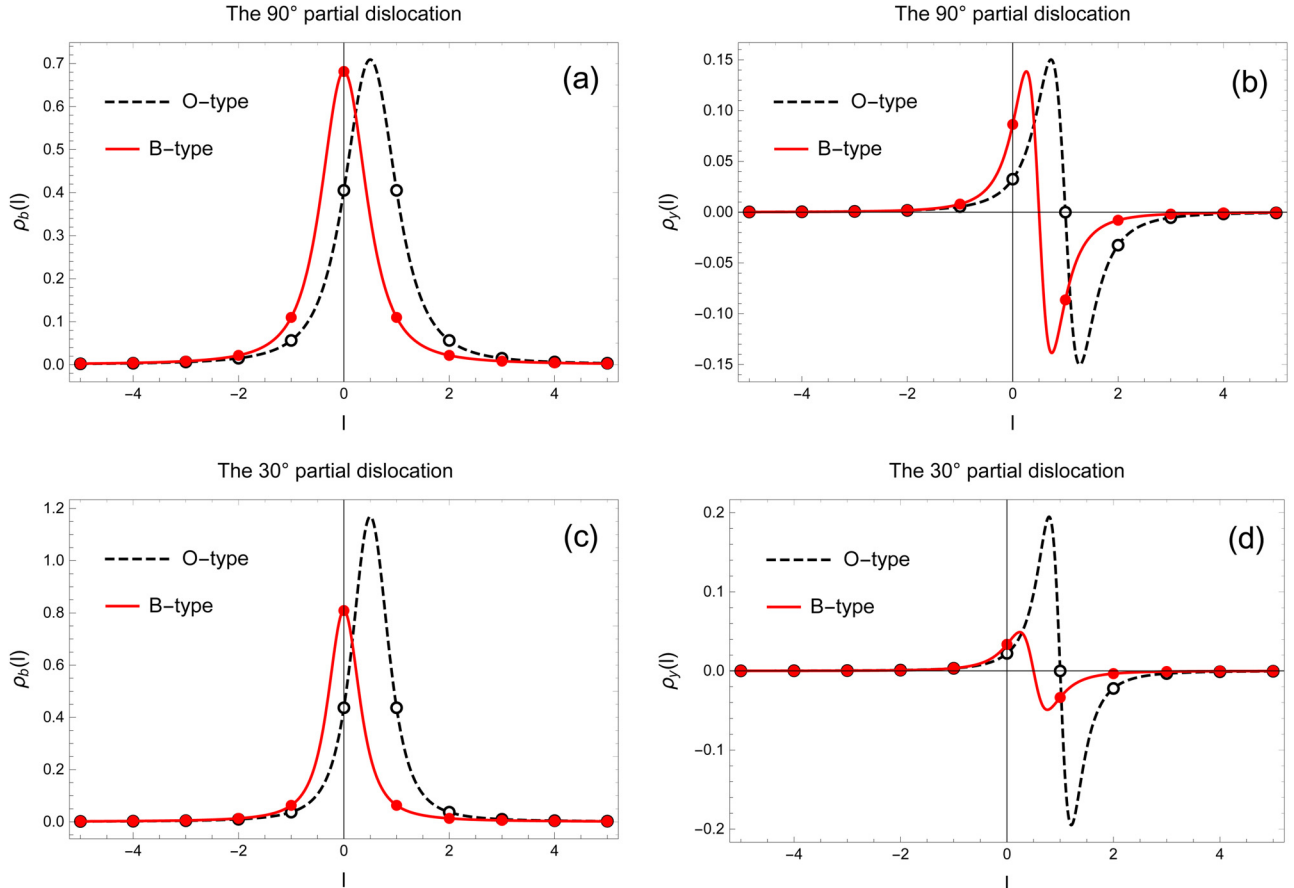

FIG. 2. Distributions of dislocation density: (a) density distribution along the slip direction $\hat{b}$ of the 90° partial dislocation; (b) density distribution related to the space varying of the 90° partial dislocation; (c) and (d) are plotted for the 30° partial dislocation.

TABLE IV. The Peierls barrier E_p and the Peierls stress σ_p.

	E_p(eV/Å)	σ_p(eV/Å^3)(Gpa)
90° partial	0.012	0.005 (0.80)
30° partial	0.043	0.018 (2.89)

named as the B-type core (B-core) and the O-type core (O-core). A dislocation with different core has different energy. The equilibrium core with the lowest energy is stable one. The two types of dislocation are distinct from each other not only in the configuration structure, but also in the positions of their symmetric axes. Once the dislocation is transformed from one type into the other type, it moves forward a step $\lambda/2$ that equals half a period of the Peierls periodic-potential. Therefore, two types of dislocation are at least separated by a distance $\lambda/2$. The transformation between different types implies a movement of the dislocation. The motion of a dislocation is realized through a sequence transformation between the B-type and the O-type dislocation

$$B \Rightarrow O \Rightarrow B \Rightarrow O \Rightarrow B \Rightarrow O \cdots .$$

Therefore, the energy barrier to be overcome for a moving dislocation is given by the energy difference between the B-type and the O-type dislocations, $E_p = |E_B - E_O|$. As a leading term approximation, the dislocation energy as a function of the position coordinate x_c can be written as

$$E(x_c) = \frac{1}{2}E_p\left(1 - \cos\frac{2\pi x_c}{\lambda}\right), \quad (7)$$

provided that the zero-point is suitably chosen.

The Peierls stress is an important physical quantity that characterizes mobility of a dislocation. It is the minimum stress that is needed to make a dislocation move. In the present theory, the Peierls stress is the maximum value of the derivative

$$\sigma_p = max\left|\frac{1}{b}\frac{dE}{dx_c}\right| = \frac{\pi E_p}{b\lambda}. \quad (8)$$

It is proportional to the Peierls energy and inversely proportional to the Burgers vector b and the period λ. The Peierls barrier E_p and the Peierls stress σ_p for the 90° and 30° partial dislocations in ZnS are listed in Table IV. We see that the Peierls stress of the 90° partial dislocation with the B-S-core is very small, $\sigma_p = 800MPa$, considering ZnS being a semiconductor material.

III. THE CORE STRUCTURES AND THE KINKS

As is well known, the long range feature of the dislocations makes it difficult to simulate the dislocation precisely. Usually, a periodic array of dislocation dipoles is used to overcome the long-range problem. While periodicity of the array make the numerical calculation easy in the electron
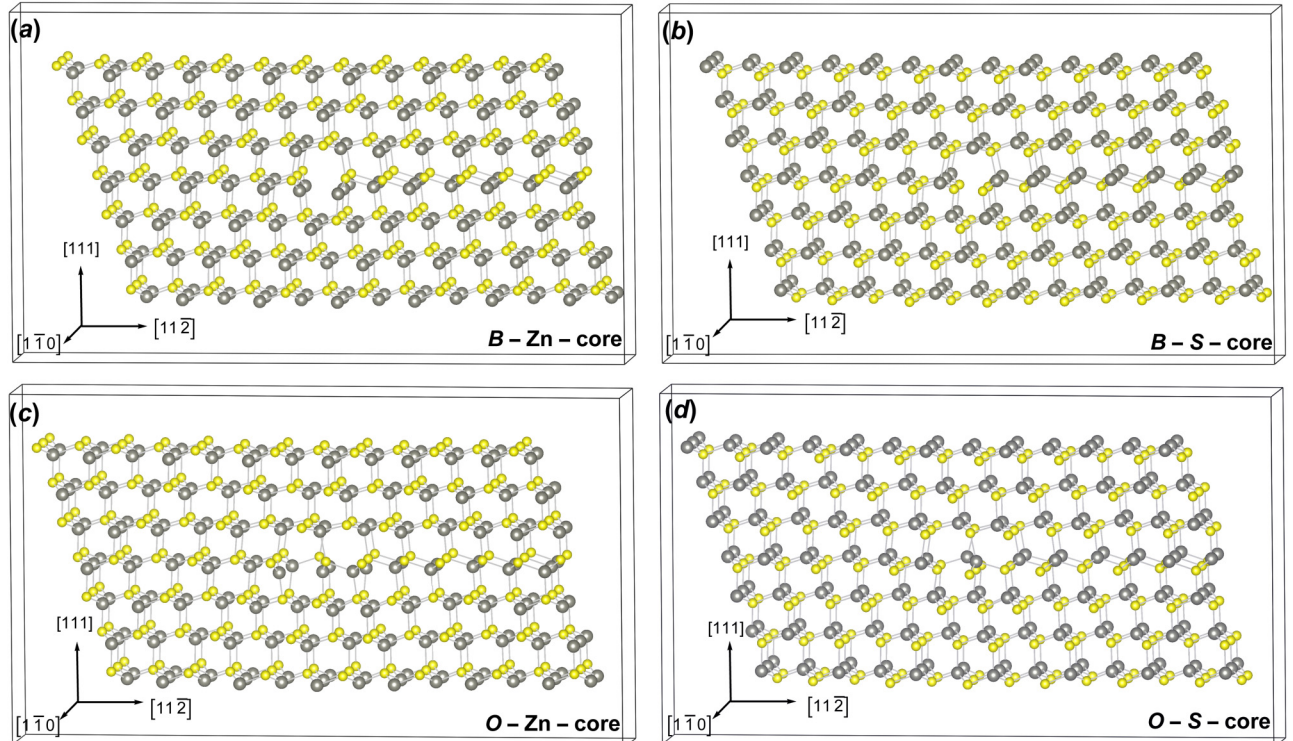

FIG. 3. The supercells and atom alignment used in *ab initio* relaxation: (a) B-Zn-core, (b) B-S-core, (c) O-Zn-core, and (d) O-S-core. The dislocation line lies along the [1$\bar{1}$0] direction. In order to eliminate the effect of polar surface as far as possible, the surfaces are chosen to be paired {111} plane, which has a relatively small polar moment because the space between two paired plane is small.
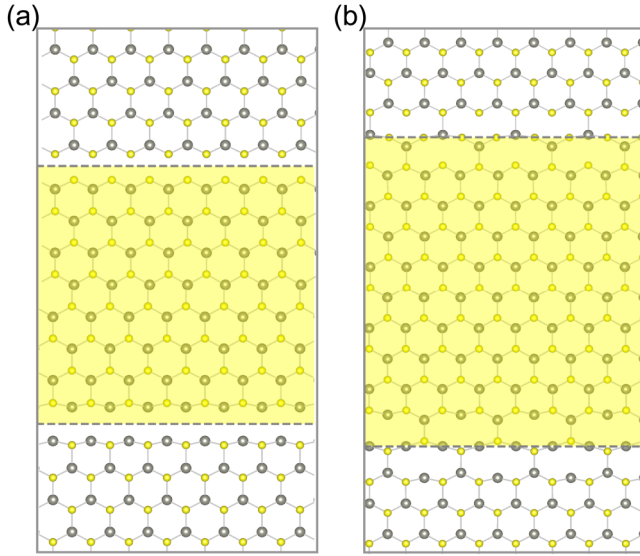
FIG. 4. The four different cores of 90° partial dislocation: (a) B-S-core (upper one) and B-Zn-core (lower one); (b) O-S-core (upper one) and O-Zn-core (lower one). The shadow area is a stacking-fault band. In a sense, the B-S-core (O-S-core) can be viewed as the anti-core of the B-Zn-core (O-Zn-core) because they will annihilate if they meet together.

density functional theory; however, the interaction between the dislocation and anti-dislocation may make the real core structure different from that of an isolated dislocation. Here, instead of dipole array, we use a prism with a rectangle cross section containing the dislocation core to perform the first-principles relaxation with VASP package.[23,24] The prism has a period $2 \times c$ ($c = 3.85$ A, the lattice period along the dislocation line) in the axis direction to allow the dimer reconstruction. The supercells, which is a rectangular slab with thickness $2c$, and atom alignment in each supercell are shown in Fig. 3. The atom configuration in the $(1\bar{1}0)$ plane is composed of 14 $\langle 11\bar{2} \rangle$-chains aligned in the $\langle 111 \rangle$ direction,
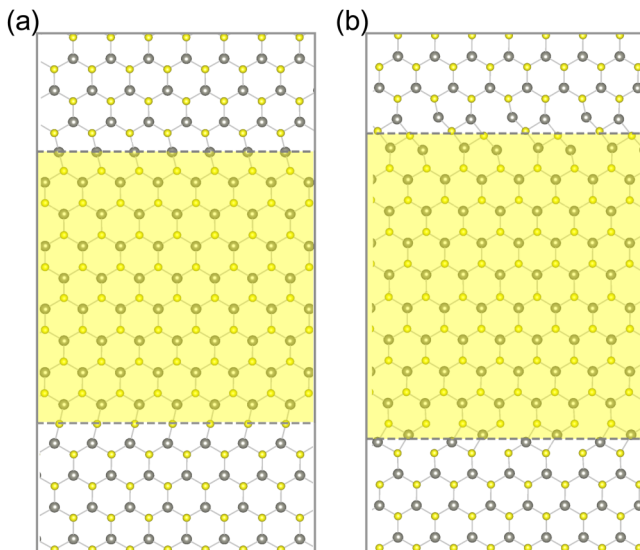

FIG. 5. The four different cores of 30° partial dislocation: (a) B-Zn-core (upper one) and B-S-core (lower one); (b) O-S-core (upper one) and O-Zn-core (lower one).

the chain length is about 12λ. The thickness of the vacuum layer is taken to be 10 A. There are 364 atoms in the supercell used. Every atom in the prism is initially positioned according to the displacement field of the dislocation, which can be obtained by using the solution given in Sec. II. In the numerical calculation, boundary atoms about two layer thick are fixed and interior atoms are free to be fully relaxed. The energy cutoff is 350 eV, and the grid mesh is $5 \times 1 \times 1$. The iteration convergence is 1.0×10^{-5} eV and 1.0×10^{-2} eV/A for the energy and the force, respectively.

It is very important to notice that in the first principle calculations using vacuum layers for materials with ionic nature requires close attention. In our calculation, we use the following method to make the results reliable. Firstly, in order to eliminate the effect of polar surface as far as possible, the surfaces are chosen to be paired {111} plane, which has a relatively small polar moment because the space between two paired planes is very small. The surface plane looks neutral if the distance is far enough. Secondly, the core structures and related energy are confirmed by converging examinations, including convergence in the supercell size effect and the charged surface effect.

We find that there are four equilibrium cores for the 90° partial dislocation and for the 30° partial dislocation. In viewpoint of fully discrete theory, the reason is simple. Because the lattice structure of sphalerite ZnS is complex one, each B-type (O-type) dislocation splits into two: one is called Zn-core to which the inmost atoms at the core are zinc atoms and the other is called S-core to which the inmost atoms at the core are sulfur atoms. Therefore, it is rational to name the four different cores as B-Zn-core, B-S-core, O-Zn-core, and O-S-core. The equilibrium cores are shown in Figs. 4 and 5 for the 90° partial dislocation and for the 30° partial dislocation. The related core energy is presented in Table V. For the 90° partial dislocation, the O-Zn-core has the lowest energy. When this O-Zn-core moves through crystal, it periodically transform into the B-Zn-core

$$\text{O-Zn} \Rightarrow \text{B-Zn} \Rightarrow \text{O-Zn} \Rightarrow \text{B-Zn} \Rightarrow \text{O-Zn} \Rightarrow \text{B-Zn} \cdots.$$

Obviously, the energy difference between the B-Zn-core and O-Zn-core is the height of the Peierls barrier

$$E_p = E_{B-Zn} - E_{O-Zn} = 0.11 \text{ eV/c} = 0.029 \text{ eV/A}.$$

It is noted that for the 90° partial dislocation, the Zn-core and S-core cannot transform each other. To understand this point clearly, it is crucial to see (Fig. 4) that the S-core is

TABLE V. Energy of the partial dislocations with different equilibrium cores in unit of eV/c, ΔE is the difference of energy between the S-core and the Zn-core.

	90° partial			30° partial		
	Zn − core	S − core	ΔE	Zn-core	S-core	ΔE
B-type (relax)	−587.36	−587.15	0.21	−586.07	−586.32	−0.25
O-type (recon)	−587.45	−587.11	0.34	−586.48	−585.94	0.54

TABLE VI. The stable partial dislocations and their Peierls barrier in unit of eV/c.

90° partial	30° partial
B-S-core 0.04	B-Zn-core 0.13
O-Zn-core 0.11	O-Zn-core 0.16

actually the anti-core of the Zn-core for the 90° partial dislocation. Any core cannot transform into its anti-core except the anti-core is identified to itself (identical transformation). Because the inmost atom at the core is invariant for the 90° partial dislocation, we conclude that the B-S-core is also a stable one although its energy is not the lowest. The Peierls barrier of the B-S-core is

$$E_p = E_{O-S} - E_{B-S} = 0.04\,\text{eV/c} = 0.01\,\text{eV/A}.$$

This is a very small barrier for a semiconductor material. Its value is closed to the prediction obtained from analytical theory. For the 30° partial dislocation, the O-Zn-core still has the lowest energy. However, when this O-Zn-core moves through crystal, it periodically transform into the B-S-core

$$\text{O-Zn} \Rightarrow \text{B-S} \Rightarrow \text{O-Zn} \Rightarrow \text{B-S} \Rightarrow \text{O-Zn} \Rightarrow \text{B-S} \cdots.$$

As a result, the height of the Peierls barrier is the energy difference between the B-S-core and O-Zn-core

$$E_p = E_{B-S} - E_{O-Zn} = 0.16\,\text{eV/c} = 0.042\,\text{eV/A}.$$

In addition, similar to the discussion for the 90° partial dislocation, we can see that the B-Zn-core of the 30° partial dislocation is also a stable one although its energy is even larger than that of the B-S-core. The Peierls barrier is

$$E_p = E_{O-S} - E_{B-Zn} = 0.13\,\text{eV/c} = 0.034\,\text{eV/A}.$$

Once again, we find that the activation energy of the B-S-core of the 90° partial dislocation is much smaller than that of the others. Furthermore, it is observed that the O-core has a doubled-period and the B-core has a single-period.

In Table VI, the stable cores and their Peierls barrier are listed for the 90° and 30° partial dislocations. In addition to these stable cores, there are four unstable equilibrium cores (some of them may be metastable due to the trap barrier resulting from the core reconstruction). Because a moving dislocation periodically transforms from the stable core to the unstable core, each stable core has a particular unstable core as its partner. For example, the unstable B-Zn-core is the partner of the O-Zn-core for the 90° partial dislocation. The existence of the unstable partner enables us to introduce the concept of the partial kink. If half a dislocation is transformed into its partner, we have a partial kink. The step height of a partial kink is half a period. Similar to the kink, when the partial kink at the left side is called partial left kink, the partial kink at the right side will be called partial right kink. In Fig. 6(b), a partial kink pair consisted of the left partial kink and the right partial kink is presented. Obviously, it is the minimum partial kink pair because there is one single unstable cell. As shown in Figs. 6(a) and 6(b), a minimum partial kink pair can be produced by one-step hopping of the atom A. Apparently, growth of the partial kink pair can be realized by hopping of the subsequent atom (neighboring to the atom A). Furthermore, as shown in Figs. 6(b) and 6(c), the minimum partial kink pair evolves into a global kink pair after one-step hopping of the atom B located at the top of a partial kink. Therefore, formation process of a kink pair consists of two steps: one step is formation of the intermediate state characterized by the partial kink pair; the other step is transition from the partial kink pair to the kink pair. For the O-Zn-core for the 90° partial dislocation, each individual step only involves one-step hopping of an atom. As a result, it is reasonable to believe that the activation energy involved in the kink process is not large. In Fig. 7, for the 30° partial dislocation, the partial kink pair of the stable O-Zn-core is shown, and formation process of the kink pair is presented on the atomic scale as for the case of the 90° partial dislocation. In contrast to the 90° partial dislocation, two atoms hopping occurs in the process of kink formation.

Based on the above discussion, we proposed a minimum energy path of the kink nucleation. The detail of the minimum energy path is explained in Figs. 8 and 9. Firstly, a partial kink pair is excited from the stable core. Then, the partial kink pair evolves into a kink pair and the kink pair grows up under the influence of temperature and applied stress. The partial kinks play a key role in the mechanism because the minimum energy path is characterized by birth and growth of the partial kinks. As shown in Figs. 8(c)–8(e) and 9(c)–9(e), the migration of kinks that determine the growth rate of the global kink pair is also dominated by the birth of the partial kinks. We know that kinks have their equilibrium positions of lowest energy at intervals of constant length ℓ along the dislocation. When a kink migrates from one position to a neighbor one, it must overcome an activation-energy barrier W. The kink mobility at
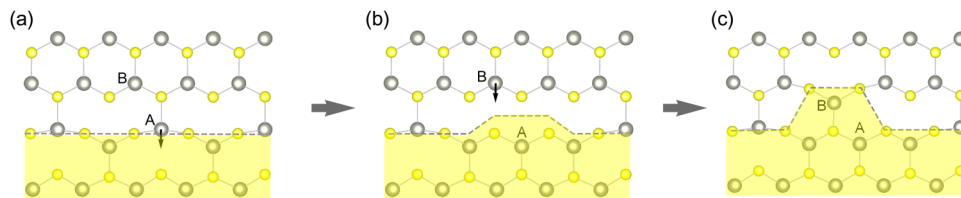

FIG. 6. Illustration of formation of a pair of kink and anti-kink in the O-S-core of the 90° partial dislocation. (a) The ground state of the O-S-core; (b) after hopping of the atom A in (a), a minimum pair of the partial kink and anti-kink appears; (c) after hopping of the atom B in (b), the partial kink pair transits into the kink pair. The symmetric center-position moves a distance $c/2$ in the process.
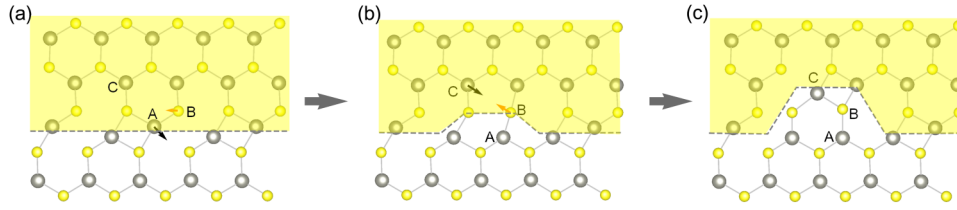
FIG. 7. Formation of a pair of kink and anti-kink in the O-Zn-core of the 30° partial dislocation. The process is similar to Fig. 6 except that two atom hopping takes place.

temperature T is[21]

$$\alpha = \frac{\nu_D \ell^2}{kT} e^{-\frac{W}{kT}},$$

where ν_D is the Debye frequency. From the migration process revealed in Figs. 8(c)→8(d)→8(e) [or Figs. 9(c)→9(d)→9(e)], we see that at the intermediate (transition) state from one equilibrium position to the neighbor position, a global

kink is dissociated into two partial kinks separated by a minimum unstable cell. If we assume the energy of two partial kinks approximately equal to that of a global kink, we obtain

$$W \approx c E_P,$$

the activation-energy barrier W equals the excitation energy of a dislocation segment of length c. In addition, it is noticed that instead of the intrinsic period of crystal, the step length of kink migration is $\ell = 2c$. The reason is that the dislocation core is reconstructed to be doubled-period one. Now,
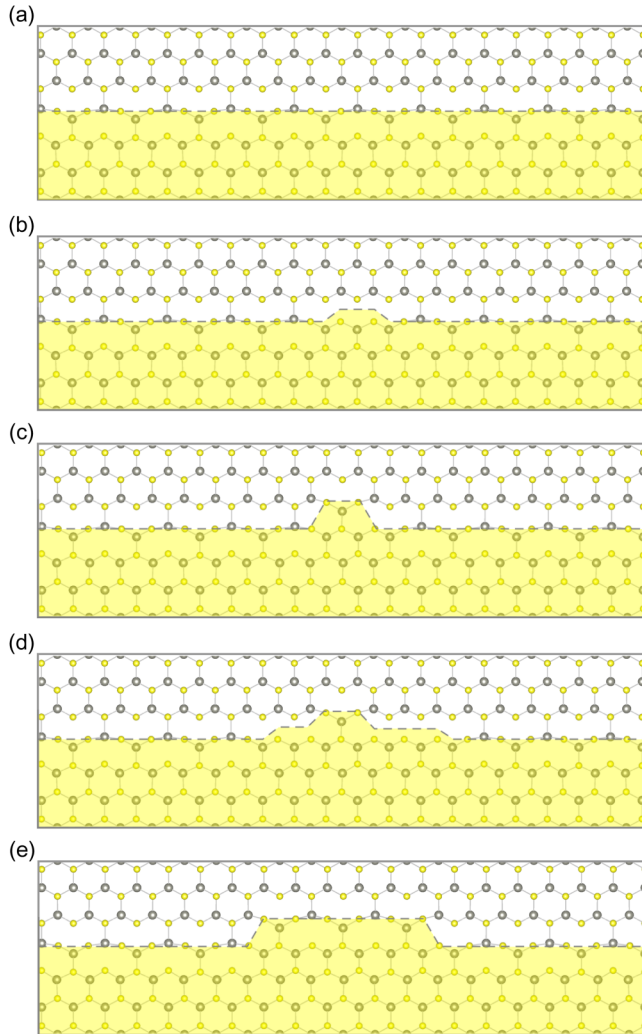

FIG. 8. The microscopic process of the formation and growth of a pair of kink and anti-kink in the O-S-core of the 90° partial dislocation. (a) The ground state of the O-S-core; (b) a cell of the B-S-core (minimum repeated unit of the B-S-core), which is the minimum pair of the partial kink and anti-kink; (c) the partial-kink pair evolves into the kink pair when the Zn atom on the top (left-corner or right-corner) of the cell takes a hopping downward; (d) two new partial kinks appear as the intermediate state and the partial left-kink and the partial right-kink are not symmetrical; (e) a large kink-pair with five cells appears, which implies that the step length of kink migration is doubled.
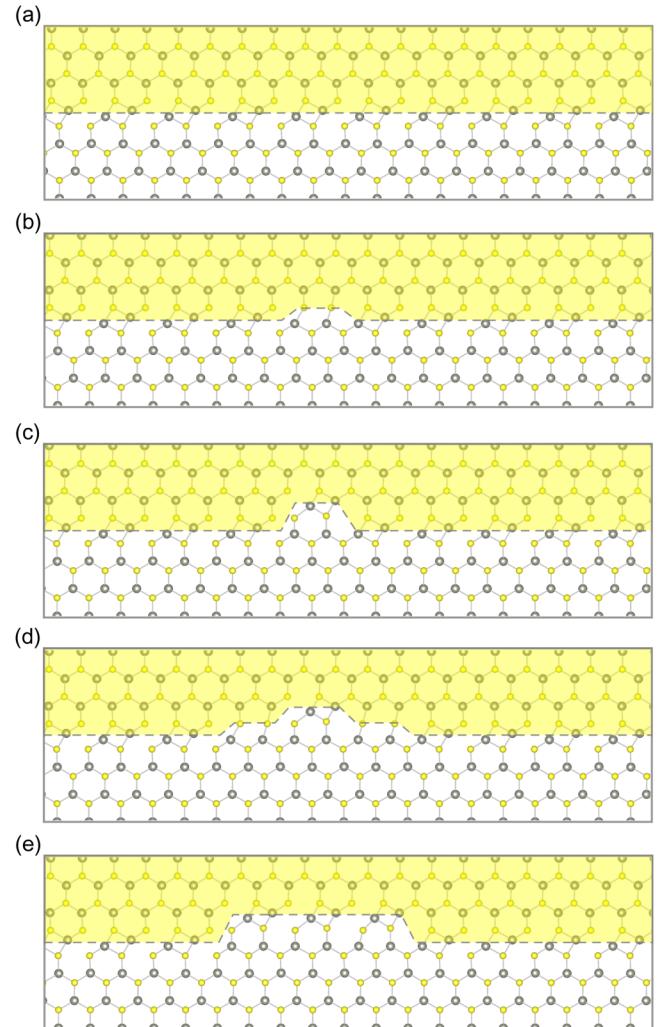

FIG. 9. The microscopic process of the formation and growth of a pair of kink and anti-kink in the O-Zn-core of the 30° partial dislocation. (a) The ground state of the O-Zn-core; (b) a cell of the B-S-core; (c) the partial-kink pair evolves into the kink pair when the Zn atom on the top (left-coner or right-corner) of the cell takes a hopping downward; (d) two new partial kinks appear; (e) a large kink-pair.

we can conclude that the kink mobility can be approximately written as

$$\alpha \approx \frac{4\nu_D c^2}{kT} e^{-\frac{cE_p}{kT}}. \tag{9}$$

This equation found the relation between the kink mobility of the energy of the unstable dislocation core.

IV. SUMMARY

The 90° and 30° partial glide dislocations in ZnS are investigated theoretically in the framework of the fully discrete Peierls model and first-principles calculations. It is found that there are four types of equilibrium cores for each kind of partial glide dislocation. In the four types of equilibrium cores, two of them are stable. And each stable core has an unstable core as its partner. For the 90° partial dislocation, the O-Zn-core (double-period core) and the B-S-core (single-period core) are stable. The Peierls barrier heights of the O-Zn-core and the B-S-core, respectively, are about 0.03 eV/A and 0.01 eV/A. For the 30° partial dislocation, the O-Zn-core (double-period core) and the B-Zn-core (single-period core) are stable and their Peierls barrier heights are approximately the same as that of the O-Zn-core of the 90° partial dislocation. Polymorphism of dislocation core structures at the atomic scale was discussed previously by Wang et al.[5,25–27] We hope that stable core doublets predicted here can be confirmed in experiment. The Peierls stress related to the barrier height is about 800 MPa for the 90° partial dislocation with the B-S-core. This critical stress required to make a dislocation move is very small for a semiconductor material. It may be responsible for the extraordinary plasticity observed recently.[1]

The existence of the unstable equilibrium core enables us to introduce partial kinks. The partial kinks play a key role in the nucleation mechanism because the minimum energy path is characterized by excitation of the partial kinks. The minimum energy path of kink migration may be verified by molecule dynamical simulation.

[1]Y. Oshima, A. Nakamura, and K. Matsunaga, Science **360**, 772 (2018).
[2]A. V. Zaretskii, Y. A. Osipyan, V. F. Petrenko, G. K. Strukova, and I. I. Khodos, Philos. Mag. A **48**, 279 (2006).
[3]J. R. Chelikowsky and J. C. H. Spence, Phys. Rev. B **30**, 694 (1984).
[4]V. F. Petrenko and R. W. Whitworth, Philos. Mag. A **41**, 681 (1980).
[5]Z. Wang, M. Saito, K. P. McKenna, and Y. Ikuhara, Nat. Commun. **5**, 3239 (2014).
[6]J. W. Christian and V. Vítek, Rep. Prog. Phys. **33**, 307 (1970).
[7]J. Bennetto, R. W. Nunes, and D. Vanderbilt, Phys. Rev. Lett. **79**, 245 (1997).
[8]R. W. Nunes, J. Bennetto, and D. Vanderbilt, Phys. Rev. B **57**, 10388 (1998).
[9]R. W. Nunes and D. Vanderbilt, Phys. Rev. B **85**, 3540 (2000).
[10]R. W. Nunes and D. Vanderbilt, J. Phys.: Condens. Matter **12**, 10021 (2000).
[11]S. Wang, L. Huang, and R. Wang, Acta Mater. **109**, 187 (2016).
[12]D. Berlincourt, H. Jaffe, and L. R. Shiozawa, Phys. Rev. **129**, 1009 (1963).
[13]R. Casali and N. Christensen, Solid State Commun. **108**, 193 (1998).
[14]T. V. Anil, C. S. Menon, K. Shree Krishna Kumar, and K. P. Jayachandran, J. Phys. Chem. Solids **65**, 1053 (2004).
[15]E. Güler and M. Güler, Braz. J. Phys. **45**, 296 (2015).
[16]R. Khenata et al., Comp. Mater. Sci. **38**, 29 (2006).
[17]X.-R. Chen, X.-F. Li, L.-C. Cai, and J. Zhu, Solid State Commun. **139**, 246 (2006).
[18]R. Peierls, Proc. Phys. Soc. **52**, 34 (1940).
[19]F. R. N. Nabarro, Proc. Phys. Soc. **59**, 256 (1947).
[20]S. Wang, S. Li, and R. Wang, Eur. Phys. J. B **83**, 15 (2011).
[21]J. P. Hirth and J. Lothe, Theory of Dislocations, 2nd ed. (Wiley, New York, 1982).
[22]S. Wang, H. Zhang, X. Wu, and R. Liu, J. Phys. Condens. Matter **22**, 055801 (2010).
[23]G. Kresse and J. Hafner, Phys. Rev. B **47**, 558 (1993).
[24]G. Kresse, Phys. Rev. B **54**, 11169 (1996).
[25]R. Sun, Z. Wang, M. Saito, N. Shibata, and Y. Ikuhara, Nat. Commun. **6**, 7120 (2015).
[26]T. Fu et al., Appl. Surf. Sci. **357**, 643 (2015).
[27]T. Fu et al., Sci. Rep. **6**, 35665 (2016).